Energy Landscape Design Principle for Optimal Energy Harnessing by Catalytic Molecular Machines

Zhongmin Zhang, Vincent Du, and Zhiyue Lu*
Department of Chemistry, University of North Carolina, Chapel Hill, NC 27599-3290, U.S.A.

Under temperature oscillation, cyclic molecular machines such as catalysts and enzymes could harness energy from the oscillatory bath and use it to drive other processes. Using a novel geometrical approach, under fast temperature oscillation, we derive a general design principle for obtaining the optimal catalytic energy landscape that can harness energy from a temperature-oscillatory bath and use it to invert a spontaneous reaction. By driving the reaction against the spontaneous direction, the catalysts convert low free energy product molecules to high free energy reactant molecules. The design principle, derived for arbitrary cyclic catalysts, is expressed as a simple quadratic objective function that only depends on the reaction activation energies, and is independent of the temperature protocol. Since the reaction activation energies are directly accessible by experimental measurements, the objective function can be directly used to guide the search for optimal energy-harvesting catalysts.

In stochastic thermodynamics, catalysts and enzymes can be considered cyclic molecular machines [1–10]: the catalyst undergoes a cycle of state changes to assist the conversion of reactant(s) to product(s), and returns to its initial state. In a stationary environment, the catalytic cycle reaches a nonequilibrium steady state (NESS), driven by the thermodynamically spontaneous reaction ($\Delta G < 0$) to a biased direction.

In idealized stationary environments, molecular machines can transduce free energy from one form to another [11–13]. By contrast, molecular machines in realistic time-varying environments can demonstrate novel dynamical and thermodynamic behavior beyond NESS. For example, a periodically oscillating environment could drive a detailed-balanced system to mimic a dissipative system [14, 15]. Moreover, the driving force provided by the time-changing environment could drive enzymes or molecular complexes to function as engines, ratchets, or pumps [16–28]. Also, periodically oscillating temperatures could drive catalysts to alter the reaction kinetics or even shift the equilibrium concentration [29–32]. These results indicate that catalysis could also demonstrate novel behavior in time-varying environments.

Many existing works on molecular ratchet focus on their dynamics with a given fixed energy landscape [10, 22, 27, 28, 33–41]. However, only recently people started to explore the *optimal design of the energy landscape* for functional molecular ratchets and pumps [42–45]. This work focuses on identifying a novel regime of driven catalysis and the corresponding design principles of its optimal energy landscape.

Consider a catalyst and a chemical reaction whose forward direction is always spontaneous for a continuous range of stationary temperatures. If temperature oscillates within the range, can the catalyst drive the reaction backward? If yes, the catalyst harnesses environmental energy to convert low free energy products to high free energy reactants. Although counter-intuitive, this effect is similar to the Parrondo's Paradox [46], where a gambler can win a game by periodically switching between two losing strategies.

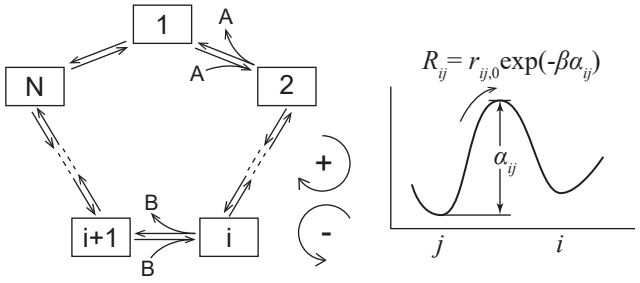

FIG. 1. A general model of a catalyzed reaction, where the catalyst undergoes a cyclic pathway consisting of N intermediate states and $2N$ transitions. A and B represent the sets of reactants and products, which can join/leave the catalytic loop at arbitrary locations. We choose a convention that the forward reaction goes clockwise. The transition from j to i and its rate $R_{ij}$is illustrated by the energy landscape.

This letter derives a universal objective function to find catalyst's energy landscape that can maximally drive the reaction against its spontaneous direction. The objective function (Eq. 13) is simply related only to the activation energies in the catalytic cycle, shown as α_{ij} in Fig. 1. Thus, this theory is directly applicable to experimental selections of catalysts or designing catalytic reaction pathways to achieve energy harvesting.

Consider a general Markov model of the cyclic kinetics of catalysis sketched in Fig. 1, as a single-loop catalytic pathway consisting of N states. By completing a cycle, the reactant A is converted into product B, and the catalyst returns to its initial state. There are $2N$ transitions on the N-state cycle between adjacent states whose rates follow the Arrhenius law,

$$R_{ij} = r_{ij,0}\exp(-\beta\alpha_{ij}) \tag{1}$$

for state j to i. Here β is the inverse temperature, and

* zhiyuelu@unc.edu

α_{ij} is the activation energy of the transition from j to i (see Fig. 1). The temperature-independent prefactor, $r_{ij,0}$, can be proportional to the concentration of external molecule (A or B) if an external molecule is absorbed in the transition.

The dynamics of the catalysis can be described by the master equation

$$\frac{\mathrm{d}\vec{p}}{\mathrm{d}t} = \hat{R}(\beta)\cdot\vec{p} \tag{2}$$

where $\vec{p}$ is a N-dim column vector characterizing the probability of each state, $\hat{R}(\beta)$ is the transition rate matrix at given inverse temperature β, the off-diagonal elements of $\hat{R}$ is R_{ij}, and the diagonal elements are chosen such that each column of $\hat{R}$ sums to 0.

Throughout this paper, we assume that the chemical bath is infinitely large, so the chemical concentrations remain constant. Then at a fixed temperature, this system reaches a NESS, $\vec{p}^{\,ss}$ where $\hat{R}(\beta)\cdot\vec{p}^{\,ss} = 0$. Then spontaneous reaction's rate is characterized by the net NESS probability current:

$$J^{ss} = R_{21}p_1^{ss} - R_{12}p_2^{ss} \tag{3}$$

where at NESS, the current is uniform across the loop, and we choose to define it between states 1 and 2. In this work, we choose the convention that clockwise (CW) current is positive, corresponding to the forward reaction (A to B), and the counter-clockwise (CCW) current is negative. If the Gibbs free energy of A is higher than B ($G_A > G_B$), the forward reaction is spontaneous, leading to a positive NESS current $J^{ss} > 0$. The affinity, which is equal to the free energy difference between A and B, determines the direction:

$$\mathcal{A} \equiv \beta^{-1}\sum_{\langle i,j\rangle}\varepsilon_{ij}\ln R_{ij} = G_A - G_B = -\Delta G \tag{4}$$

where ΔG is the free energy change corresponding to the forward reaction, the $\sum_{\langle i,j\rangle}$ sums over all of the $2N$ transitions from j to i on the loop. We have adopted the following sign indicator of transition from j to i:

$$\varepsilon_{ij} = \begin{cases} 1 & \text{forward} \\ -1 & \text{backward} \end{cases} \tag{5}$$

If $\mathcal{A} > 0$, the spontaneous reaction is forward, $\mathcal{A} < 0$ backward, and if $\mathcal{A} = 0$, the system is at thermal equilibrium without net reaction flow. In this paper, we assume G_A is always greater than G_B within the temperature range of interest, and thus $\mathcal{A} > 0$ and $J^{ss} > 0$, and the spontaneous reaction always goes forward (CW).

If the temperature non-quasi-statically oscillates in time, the chemical reaction is driven out of NESS. The system eventually reaches a time-periodic state (i.e., a periodic orbit in probability space): $\vec{p}(t+\tau) = \vec{p}(t)$, where τ is period of temperature oscillation. There have been studies of the periodic states under periodic temperature modulation [29–31]. However, it is generally impossible to analytically solve the dynamics for arbitrary systems or arbitrary reaction landscapes. To derive the generic design principle, in this letter, we consider the *fast oscillation limit* $\tau \to 0$ [47], where a perturbation analysis [48] for small periods τ could reveal an analytical solution of the periodic orbit shrinking into a fixed point $\vec{p}(t) \to \vec{p}^{\,*}$, which leads to a general principle that applies to arbitrary reaction energy landscapes. (See SI.I [49]) The fixed point $\vec{p}^{\,*}$ can be considered as an *effective NESS* corresponding to an *effective rate matrix* $\hat{R}^*$:

$$\hat{R}^*\cdot\vec{p}^{\,*} = 0 \tag{6}$$

where the effective rate matrix is nothing but the time average of $\hat{R}(\beta(t))$ over a period:

$$\hat{R}^* \equiv \lim_{\tau\to 0}\frac{1}{\tau}\int_0^\tau \hat{R}(\beta(t))\mathrm{d}t \tag{7}$$

At the fast oscillation limit, one can find the average current by using $\vec{p}^{\,*}$ and $\hat{R}^*$ similar to that in Eq. 3:

$$J^* = {R^*}_{21}p_1^* - {R^*}_{12}p_2^* \tag{8}$$

In contrast to NESS, the affinity is no longer well-defined since the temperature is no longer a fixed constant. Here without a constant temperature, we introduce an *dimensionless affinity*,

$$\tilde{\mathcal{A}} = \sum_{\langle i,j\rangle}\varepsilon_{ij}\ln R_{ij} \tag{9}$$

where R_{ij} is not restricted to a fixed-temperature rate matrix $\hat{R}(\beta)$ but can also be defined for effective rate matrix $\hat{R}^*$. At a constant temperature, the $\tilde{\mathcal{A}}$ calculated from stationary temperature rate matrix $\hat{R}(\beta)$ can be related back to $\mathcal{A}$ by $\tilde{\mathcal{A}} = \beta\mathcal{A}(\beta) = -\beta\Delta G$. When temperature rapidly oscillates, one can define the effective dimensionless affinity $\tilde{\mathcal{A}}^*$ by plugging the effective rate matrix $\hat{R}^*$ in Eq. 9.

Under oscillatory temperature, the direction of reaction (the sign of J^*) is solely determined by the active driving force $\tilde{\mathcal{A}}^*$: if $\tilde{\mathcal{A}}^* > 0$, the reaction on average proceeds forward ($J^* > 0$); if $\tilde{\mathcal{A}}^* < 0$, the reaction on average proceeds backward ($J^* < 0$).

Thus, the goal of searching for a catalyst to invert a spontaneous reaction is formulated in terms of $\tilde{\mathcal{A}}^*$: Consider a spontaneous reaction where $\Delta G < 0$, $J(\beta) > 0$, and $\tilde{\mathcal{A}}(\beta) > 0$ for any temperature within a continuous range. When temperature oscillates within the range, what catalyst facilitates a negative $\tilde{\mathcal{A}}^* < 0$ (i.e., reaction is inverted and $J^* < 0$)?

In this letter, based on the geometric property of $\tilde{\mathcal{A}}$, we obtain a universal objective function, Eq. 13, to find the optimal catalytic reaction inversion. Historically, geometry has played important roles in thermodynamics. Gibbs first used geometry to demonstrate the thermodynamic properties within the space of state functions [50]. Recently, Crooks [51], Ito [52, 53], and Dong [54] have derived various general thermodynamic results by utilizing

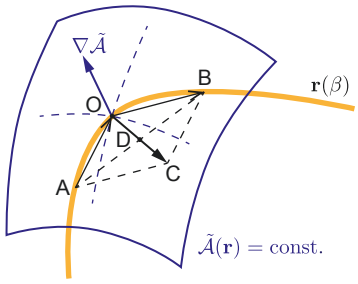

FIG. 2. Illustrated is the 2N-dimensional design space of $\mathbf{r} = (R_{21}, R_{12}, ..., R_{ji}, R_{ij}, ..., R_{1N}, R_{N1})$. The yellow β-locus crossing 3 points AOB is the set of $\mathbf{r}(\beta)$ corresponding to a given energy landscape at all possible inverse temperature β's. Blue surface represents a $(2N-1)$-manifold defined by $\tilde{\mathcal{A}}(\mathbf{r}) = \text{const}$ that contains point O. The gradient of $\tilde{\mathcal{A}}(\mathbf{r})$ at point O, is shown as the blue normal vector $\nabla\tilde{\mathcal{A}}$. When we consider temperature oscillation between $\beta_{1,2} = \beta_0 \pm \Delta\beta$, their corresponding rate matrices are points A and B. The rate matrix at β_0 is represented by point O. The effective rate matrix $\hat{R}^*$ corresponds to the midpoint D between A and B. At infinitesimal temperature amplitude, the vector $\overrightarrow{\text{OC}} = \overrightarrow{\text{OB}} - \overrightarrow{\text{AO}}$ becomes $\mathrm{d}^2\mathbf{r}\,/\,\mathrm{d}\beta^2$ in Eq. 11.

differential geometry within various types of probability-distribution spaces.

Rather than working within a probability space, this letter focuses on the geometry in the $2N$-dimensional space consisting of kinetic rates: $\mathbf{r} = (R_{21}, R_{12}, ..., R_{ji}, R_{ij}, ..., R_{1N}, R_{N1})$. According to Eq. 1, the reaction rates are determined by both temperature β^{-1} and the catalytic energy landscape α_{ij}'s. For any catalyst specified by its energy landscape α_{ij}'s, its kinetic rates $\mathbf{r}(\beta)$ parameterized by inverse temperature β is illustrated by a yellow β-locus in Fig. 2.

Without losing generality, let us illustrate our theory using a simple square-wave temperature oscillation between β_1 and β_2 of equal time duration. At constant temperature, β_1 (or β_2), the kinetic rate matrix $\hat{R}(\beta)$ or equivalently $\mathbf{r}(\beta)$ is illustrated by the point A (or B) on the β-locus in Fig. 2. Under fast temperature oscillation, the effective rate matrix is simply the arithmetic mean:

$$\hat{R}^* = \frac{\hat{R}(\beta_1) + \hat{R}(\beta_2)}{2} \tag{10}$$

and is represented by point D, the midpoint between A and B in the $\mathbf{r}$ space.

Recall that the generalized dimensionless affinity $\tilde{\mathcal{A}}(\mathbf{r})$ is a function on the $\mathbf{r}$-space, and its sign dictates the direction of averaged flow. By construction, within the range of $\beta \in [\beta_1, \beta_2]$, the reaction free energy $\Delta G(\beta) < 0$ and $\tilde{\mathcal{A}}(\mathbf{r}(\beta)) > 0$. Typically point D is not on the yellow locus $\mathbf{r}(\beta)$. Thus $\tilde{\mathcal{A}}(\mathbf{r})$ at point D can take a very different value than that on the yellow locus. When $\tilde{\mathcal{A}}(\mathbf{r}) < 0$ at point D, the catalyst inverts the reaction direction when temperature oscillates rapidly.

Geometrically, the catalyst is represented by a locus $\mathbf{r}(\beta)$ in the $\mathbf{r}$-space. The analysis above allows us to characterize the catalyst's ability to invert reaction by how much the locus $\mathbf{r}(\beta)$ curves toward the steepest descent direction (gradient) of $\tilde{\mathcal{A}}(\mathbf{r})$. Notice this geometrical characterization is not dependent on the specific protocol of temperature oscillation.

The qualitative geometrical argument above can be quantified by two vectors. Firstly, the bending of the β-locus $\mathbf{r}(\beta)$ can be characterized by the second order derivative vector $\mathrm{d}^2\mathbf{r}\,/\,\mathrm{d}\beta^2$ (see vector $\overrightarrow{\text{OC}}$ in Fig. 2). This curvature-like vector is the acceleration vector for the motion of point $\mathbf{r}(\beta)$ as the β varies. The entries of $\mathrm{d}^2\mathbf{r}\,/\,\mathrm{d}\beta^2$ are

$$\frac{\mathrm{d}^2 R_{ij}}{\mathrm{d}\beta^2} = \alpha_{ij}^2 R_{ij} \tag{11}$$

Secondly, the variation of $\tilde{\mathcal{A}}$ in the $\mathbf{r}$-space is characterized by the gradient vector $\nabla\tilde{\mathcal{A}}(\mathbf{r})$ (as the blue arrow in Fig. 2), whose entries are

$$\frac{\partial\tilde{\mathcal{A}}}{\partial R_{ij}} = \frac{\varepsilon_{ij}}{R_{ij}} \ . \tag{12}$$

Combining the above, the catalyst's ability to invert the reaction direction is characterized by the inner product between the second-order derivative vector $\mathrm{d}^2\mathbf{r}\,/\,\mathrm{d}\beta^2$ and the gradient vector of $\tilde{\mathcal{A}}$:

$$\mathcal{C}(\{\alpha_{ij}\}) = \nabla\tilde{\mathcal{A}} \cdot \frac{\mathrm{d}^2\mathbf{r}}{\mathrm{d}\beta^2} = \sum_{\langle i,j\rangle} \varepsilon_{ij}\alpha_{ij}^2 \tag{13}$$

which serves as a universal objective function to find the optimal catalytic energy landscape that can achieve strong reaction inversion.

An alternative derivation based on a finite-difference analysis of temperature oscillation between $\beta_0 - \Delta\beta$ and $\beta_0 + \Delta\beta$ is shown in Fig. 2 and the supporting information (see SI.II [49]). Here $\mathcal{C}(\{\alpha_{ij}\})$ is directly proportional to $\Delta\tilde{\mathcal{A}}$, the difference of $\tilde{\mathcal{A}}$ of $\hat{R}^*$ and the NESS $\tilde{\mathcal{A}}(\beta_0)$ at constant temperature β_0.

$$\Delta\tilde{\mathcal{A}} \equiv \tilde{\mathcal{A}}(\hat{R}^*) - \tilde{\mathcal{A}}(\mathbf{r}(\beta_0)) = \mathcal{C}(\{\alpha_{ij}\})\frac{\Delta\beta^2}{2} + o(\Delta\beta^2) \tag{14}$$

Due to the nice geometric property of the constant-$\tilde{\mathcal{A}}(\mathbf{r})$ manifold and the β-locus [55], the R_{ij} from Eqs. 11 and 12 cancels out, and the resulting objective function Eq. 13 takes a simple quadratic form that only depends on the activation energies of the catalyst α_{ij}'s, and is independent of the specific temperature protocol. For the same geometrical reason, $\mathcal{C}$ applies to large-amplitude temperature oscillation (see Fig. 4b).

The objective function $\mathcal{C}(\{\alpha_{ij}\})$ is directly accessible by experiment via direct measurements of the activation energies α_{ij}'s. Thus, our result (Eq. 13) provides chemists with an easy approach to predict arbitrary catalysts' ability to invert reaction direction under fast temperature oscillation.

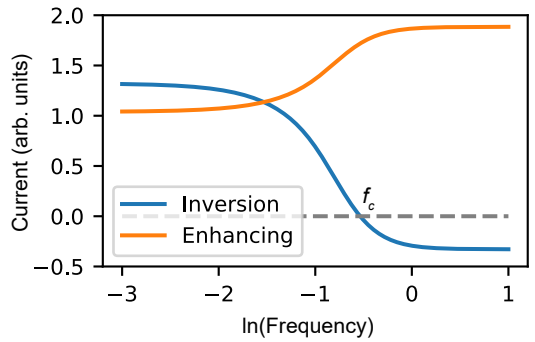

FIG. 3. Reaction rate (average probability current at periodic steady state) versus temperature oscillation frequency $f = \tau^{-1}$ for both the optimal energy landscapes for reaction inversion and enhancement, obtained for $\mathcal{A} = -\Delta G = 1$, $\alpha_{max} = 11$, $\beta_0 = 0.9$ and $\Delta\beta = 0.3$.

For illustration, Fig. 3 demonstrates the frequency response of the optimal 3-state catalyst landscape ($\{\alpha_{ij}\}$) under the following design constraints. First, we fix the reaction's free energy change $\Delta G(\beta) = -1$ for all β's. As a result, the affinity must be constant $\mathcal{A} = -\Delta G = 1$ regardless of the choice of the catalyst. Secondly, we assume that the reaction rate prefactor $r_{ij,0}$'s are all fixed to be the same constant. By doing so for any constant temperature,

$$\mathcal{A} = -\sum_{+} \alpha_{ij} + \sum_{-} \alpha_{ij} = 1 \tag{15}$$

where $\sum_+$ (or $\sum_+$) is the sum over all forward (or backward) reaction transitions. Thirdly, as we search for the optimal landscape (activation energies), we restrict the activation energies of all $2N$ transitions in the range $\alpha_{ij} \in [0, \alpha_{max}]$. Here we assume the reaction's affinity is weaker than the maximum allowed activation energy: $\mathcal{A} = 1 < \alpha_{max}$.

According to our result, to find the optimal catalyst with the strongest driving force against spontaneous reaction under temperature oscillation, one needs to minimize the objective function

$$\mathcal{C} = \sum_{+} \alpha_{ij}^2 - \sum_{-} \alpha_{ij}^2 \tag{16}$$

which is a simple quadratic minimization problem on a convex set. For $N = 3$, the optimal solution of α_{ij}'s are

$$\alpha_+^{\rm inv} = (\frac{2\alpha_{max} - 1}{3}, \frac{2\alpha_{max} - 1}{3}, \frac{2\alpha_{max} - 1}{3}) \tag{17}$$

$$\alpha_-^{\rm inv} = (\alpha_{max}, \alpha_{max}, 0) \tag{18}$$

where $\alpha_+^{\rm inv}$ are the activation energies α_{ij}'s for the 3 forward transitions and $\alpha_-^{\rm inv}$ are for the 3 backward transitions (see SI.IV [49]). The order of the 3 forward (or 3 backward) α_{ij}'s does not impact the result.

Beyond the fast oscillation limit, the optimal catalyst can invert the reaction at finite frequency f's (see Fig. 3). At the critical frequency $f = f_c$, the reaction free energy force ΔG is completely stalled by inversion force from the catalyst, and the reaction stops ($J_{\rm period} = 0$); at larger frequency, $f > f_c$ the catalyst's driving wins over ΔG and reaction direction is inverted ($J_{\rm period} < 0$). At the fast oscillation limit $f \gg 1$, we can use the Matrix Tree Theorem [56] to obtain from the effective rate matrix R^* the effective current $J^* = (R^*_{13}R^*_{32}R^*_{21} - R^*_{12}R^*_{23}R^*_{31})/\kappa$, where $\kappa > 0$ (see SI.III [49]). Thus the sign of current J^* is always the same with $\tilde{\mathcal{A}}^*$.

It is worth pointing out that the objective function Eq. 13 can be used toward an inverse effect of catalytic reaction inversion, i.e., driving force enhancing. By maximizing Eq. 13, (see SI.IV [49])

$$\alpha_+^{\rm enh} = (\alpha_{max}, \alpha_{max}, 0) \tag{19}$$

$$\alpha_-^{\rm enh} = (\frac{2\alpha_{max} + 1}{3}, \frac{2\alpha_{max} + 1}{3}, \frac{2\alpha_{max} + 1}{3}) \tag{20}$$

defines a reaction-enhancing catalyst that optimally enhances the spontaneity of a reaction. The reaction current enhanced at various frequencies f is shown in Fig. 3.

Even though $\mathcal{C}$ (Eq. 13) is obtained from the local curvature, due to nice geometric properties of $\tilde{\mathcal{A}}(\mathbf{r})$ and $\mathbf{r}(\beta)$, it remains a good optimization objective function even for big-amplitude temperature oscillations (e.g., for $\beta_0 = 0.9$, $\Delta\beta = 0.3$). We demonstrate that for both small and large amplitudes, $\mathcal{C}$ is approximately linearly correlated to the change of thermodynamic driving force. The linear correlation is shown in Fig. 4 for both small $\Delta\beta = 0.05$ and large $\Delta\beta = 0.3$ by scatter plots of 10^4 points. Each point is obtained from one randomly generated energy landscape $\{\alpha_{ij}\}$. Notice in the small amplitude limit, $\Delta\beta \ll 1$, $\mathcal{C}$ is equal to $2\Delta\tilde{\mathcal{A}}/\Delta\beta^2$ (Eq. 14). The optimal catalysts for reaction inversion and enhancement (obtained by minimizing and optimizing $\mathcal{C}$) are highlighted as red and black crosses, appearing at the two ends of both scatter plots.

At stationary temperature, kinetic intuition may argue that the higher the activation energy, the slower the corresponding transition rates. However, when temperature oscillates, our theory indicates that big variation in the activation energies of the inverse reaction direction and mild activation energies of the forward reaction direction could suppress the forward reaction and favor the inverse direction. Moreover, designing the catalytic reaction inversion suffers from a trade-off relation between strength and speed. Strong inversion (large $|\Delta\tilde{\mathcal{A}}|$) favors the choice of larger activation energies (larger α_{ij}), which impedes the net reaction current.

In conclusion, this letter demonstrated a geometric approach to derive the general design principle of optimal oscillatory-driven catalysis. In this regime, we demonstrate catalysts that can harness energy from an oscillatory-temperature bath and utilize the energy to enhance or invert a spontaneous reaction. The design

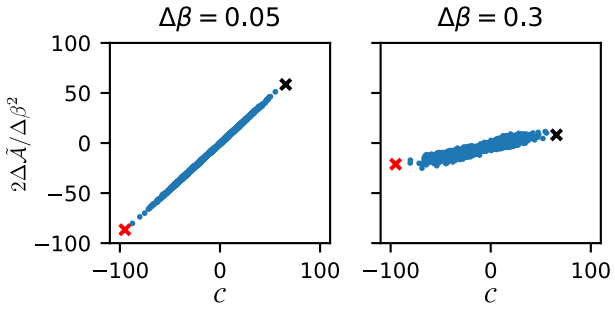

FIG. 4. Objective function $\mathcal{C}$ and the scaled affinity change $2\Delta\tilde{\mathcal{A}}/\Delta\beta^2$ for randomly generated energy landscapes under the same set restriction with the optimization problem ($\mathcal{A} = -\Delta G = 1$, $\alpha_{max} = 11$, $\beta_0 = 0.9$). The red and black crosses correspond to the optimal energy landscapes for reaction inversion (minimizing $\mathcal{C}$) and enhancement (maximizing $\mathcal{C}$).

principle is formulated by an objective function Eq. 13, which only depends on the activation energies of the energy landscape in a quadratic form. Due to the nice geometric property of the thermodynamic driving force $\tilde{\mathcal{A}}$, the objective function is independent of the temperature protocol. Moreover, this result obtained from the fast oscillation limit can still be used to invert spontaneous reactions at finite-frequency temperature oscillation. Since activation energies are accessible in the experimental study of reaction mechanisms, this result could be experimentally verified and directly used to guide the design of useful catalysts for energy harnessing.

ACKNOWLEDGMENTS

We acknowledge the financial support from the startup fund at UNC-Chapel Hill and the fund from the National Science Foundation Grant DMR-2145256. Z.L. appreciates helpful discussions with Hong Qian and suggestions on the manuscript from Chase Slowey. We also appreciate the reviewers' comments to help enhance the clarity of the presentation.

[1] H. V. Westerhoff, T. Y. Tsong, P. Chock, Y.-D. Chen, and R. Astumian, How enzymes can capture and transmit free energy from an oscillating electric field, Proceedings of the National Academy of Sciences **83**, 4734 (1986).
[2] V. Rozenbaum, D.-Y. Yang, S. Lin, and T. Tsong, Catalytic wheel as a brownian motor, The Journal of Physical Chemistry B **108**, 15880 (2004).
[3] H. Qian, Cycle kinetics, steady state thermodynamics and motors—a paradigm for living matter physics, Journal of Physics: Condensed Matter **17**, S3783 (2005).
[4] R. D. Astumian, Making molecules into motors, Scientific American **285**, 56 (2001).
[5] R. Yasuda, H. Noji, M. Yoshida, K. Kinosita, and H. Itoh, Resolution of distinct rotational substeps by submillisecond kinetic analysis of f1-atpase, Nature **410**, 898 (2001).
[6] T. L. Hill and Y.-D. Chen, Stochastics of cycle completions (fluxes) in biochemical kinetic diagrams, Proceedings of the National Academy of Sciences **72**, 1291 (1975).
[7] H. Qian, A simple theory of motor protein kinetics and energetics, Biophysical chemistry **67**, 263 (1997).
[8] H. Qian, A simple theory of motor protein kinetics and energetics. ii, Biophysical chemistry **83**, 35 (2000).
[9] R. D. Astumian and P. Hänggi, Brownian motors, Physics today **55**, 33 (2002).
[10] P. Reimann, Brownian motors: noisy transport far from equilibrium, Physics reports **361**, 57 (2002).
[11] T. L. Hill, *Free energy transduction and biochemical cycle kinetics* (Courier Corporation, 2013).
[12] Y.-D. Chen, Asymmetry and external noise-induced free energy transduction, Proceedings of the National Academy of Sciences **84**, 729 (1987).
[13] T. Tsong and R. D. Astumian, Electroconformational coupling: how membrane-bound atpase transduces energy from dynamic electric fields, Annual Review of Physiology **50**, 273 (1988).
[14] O. Raz, Y. Subaş ı, and C. Jarzynski, Mimicking nonequilibrium steady states with time-periodic driving, Phys. Rev. X **6**, 021022 (2016).
[15] D. M. Busiello, C. Jarzynski, and O. Raz, Similarities and differences between non-equilibrium steady states and time-periodic driving in diffusive systems, New Journal of Physics **20**, 093015 (2018).
[16] R. D. Astumian and M. Bier, Fluctuation driven ratchets: molecular motors, Physical review letters **72**, 1766 (1994).
[17] J. M. Horowitz and C. Jarzynski, Exact formula for currents in strongly pumped diffusive systems, Journal of Statistical Physics **136**, 917 (2009).
[18] O. Abah, J. Roßnagel, G. Jacob, S. Deffner, F. Schmidt-Kaler, K. Singer, and E. Lutz, Single-ion heat engine at maximum power, Phys. Rev. Lett. **109**, 203006 (2012).
[19] R. D. Astumian, Design principles for brownian molecular machines: how to swim in molasses and walk in a hurricane, Physical Chemistry Chemical Physics **9**, 5067 (2007).
[20] S. Rahav, J. Horowitz, and C. Jarzynski, Directed flow in nonadiabatic stochastic pumps, Physical review letters **101**, 140602 (2008).
[21] N. Sinitsyn and I. Nemenman, The berry phase and the pump flux in stochastic chemical kinetics, EPL (Europhysics Letters) **77**, 58001 (2007).
[22] R. D. Astumian, Adiabatic operation of a molecular machine, Proceedings of the National Academy of Sciences **104**, 19715 (2007).
[23] R. D. Astumian, Adiabatic pumping mechanism for ion motive atpases, Physical review letters **91**, 118102 (2003).
[24] R. D. Astumian and I. Derényi, Towards a chemically driven molecular electron pump, Physical Review Letters **86**, 3859 (2001).
[25] J. M. Parrondo, Reversible ratchets as brownian particles in an adiabatically changing periodic potential, Physical

Review E **57**, 7297 (1998).
[26] R. D. Astumian, Stochastically pumped adaptation and directional motion of molecular machines, Proceedings of the National Academy of Sciences **115**, 9405 (2018).
[27] Y.-X. Li, Transport generated by fluctuating temperature, Physica A: Statistical Mechanics and its Applications **238**, 245 (1997).
[28] P. Reimann, R. Bartussek, R. Häussler, and P. Hänggi, Brownian motors driven by temperature oscillations, Physics Letters A **215**, 26 (1996).
[29] H. Berthoumieux, L. Jullien, and A. Lemarchand, Response to a temperature modulation as a signature of chemical mechanisms, Physical Review E **76**, 056112 (2007).
[30] A. Lemarchand, H. Berthoumieux, L. Jullien, and C. Gosse, Chemical mechanism identification from frequency response to small temperature modulation, The Journal of Physical Chemistry A **116**, 8455 (2012).
[31] A. Lemarchand, H. Berthoumieux, L. Jullien, and C. Gosse, Chemical mechanism identification from frequency response to small temperature modulation, The Journal of Physical Chemistry A **116**, 8455 (2012).
[32] H. Berthoumieux, C. Antoine, L. Jullien, and A. Lemarchand, Resonant response to temperature modulation for enzymatic dynamics characterization, Physical Review E **79**, 021906 (2009).
[33] I. Derényi, M. Bier, and R. D. Astumian, Generalized efficiency and its application to microscopic engines, Physical review letters **83**, 903 (1999).
[34] I. Derényi and R. D. Astumian, Efficiency of brownian heat engines, Physical Review E **59**, R6219 (1999).
[35] B.-Q. Ai, H.-Z. Xie, D.-H. Wen, X.-M. Liu, and L.-G. Liu, Heat flow and efficiency in a microscopic engine, The European Physical Journal B-Condensed Matter and Complex Systems **48**, 101 (2005).
[36] U. Seifert, Stochastic thermodynamics, fluctuation theorems and molecular machines, Reports on progress in physics **75**, 126001 (2012).
[37] J. Parrondo and B. J. de Cisneros, Energetics of brownian motors: a review, Applied Physics A **75**, 179 (2002).
[38] K. Sekimoto, F. Takagi, and T. Hondou, Carnot's cycle for small systems: Irreversibility and cost of operations, Physical Review E **62**, 7759 (2000).
[39] T. Hondou and K. Sekimoto, Unattainability of carnot efficiency in the brownian heat engine, Physical Review E **62**, 6021 (2000).
[40] M. Asfaw and M. Bekele, Current, maximum power and optimized efficiency of a brownian heat engine, The European Physical Journal B-Condensed Matter and Complex Systems **38**, 457 (2004).
[41] C. Van den Broeck, Carnot efficiency revisited, Advances in Chemical Physics **135**, 189 (2007).
[42] A. I. Brown and D. A. Sivak, Toward the design principles of molecular machines, arXiv preprint arXiv:1701.04868 (2017).
[43] J. N. Lucero, A. Mehdizadeh, and D. A. Sivak, Optimal control of rotary motors, Physical Review E **99**, 012119 (2019).
[44] A. I. Brown and D. A. Sivak, Theory of nonequilibrium free energy transduction by molecular machines, Chemical reviews **120**, 434 (2019).
[45] A. I. Brown and D. A. Sivak, Allocating and splitting free energy to maximize molecular machine flux, The Journal of Physical Chemistry B **122**, 1387 (2018).
[46] G. P. Harmer and D. Abbott, Losing strategies can win by parrondo's paradox, Nature **402**, 864 (1999).
[47] Although the optimal design principle is derived under the fast oscillation limit, Fig. 3 indicates that the optimal catalyst here is able to invert reaction direction even under finite driving frequencies.
[48] M. Tagliazucchi, E. A. Weiss, and I. Szleifer, Dissipative self-assembly of particles interacting through time-oscillatory potentials, Proceedings of the National Academy of Sciences **111**, 9751 (2014).
[49] Supplemental Material at [URL will be inserted by publisher] for the alternative derivation of the theory and supplemental evidence.
[50] F. Weinhold, Thermodynamics and geometry, Phys. Today **29**, 23 (1976).
[51] D. A. Sivak and G. E. Crooks, Thermodynamic metrics and optimal paths, Phys. Rev. Lett. **108**, 190602 (2012).
[52] S. Ito, Stochastic thermodynamic interpretation of information geometry, Phys. Rev. Lett. **121**, 030605 (2018).
[53] K. Yoshimura and S. Ito, Information geometric inequalities of chemical thermodynamics, Phys. Rev. Research **3**, 013175 (2021).
[54] G. Li, J.-F. Chen, C. P. Sun, and H. Dong, Geodesic path for the minimal energy cost in shortcuts to isothermality, Phys. Rev. Lett. **128**, 230603 (2022).
[55] In the logarithm **r**-space, the constant-$\tilde{\mathcal{A}}$ manifolds become a set of parallel hyper-planes with unidirectional gradients, and the β-locus for any energy landscape is a straight line. The gradient of $\tilde{\mathcal{A}}$ and the acceleration vector of the β-locus has an elementary-wise inverses dependence on R_{ij}.
[56] J. Schnakenberg, Network theory of microscopic and macroscopic behavior of master equation systems, Reviews of Modern physics **48**, 571 (1976).

Supporting Information: Energy Landscape Design Principle for Optimal Energy Harnessing by Catalytic Molecular Machines

Zhongmin Zhang, Vincent Du, and Zhiyue Lu*
Department of Chemistry, University of North Carolina, Chapel Hill, NC 27599-3290, U.S.A.

I. PERTURBATION ANALYSIS IN THE FAST OSCILLATION LIMIT

Here we demonstrate that under the fast oscillation limit, the system reaches an effective steady state $\vec{p}^*$ corresponding to an effective rate matrix $\hat{R}^*$. Similar derivation for Fokker Planck equation can be found in [1].

Let us consider a time-heterogeneous Markov process described by a master equation:

$$\frac{\mathrm{d}\vec{p}(t)}{\mathrm{d}t} = \hat{R}_t\vec{p}(t) \tag{1}$$

where the transition rate matrix changes periodically in time with period τ:

$$\hat{R}_t = \hat{R}_{t+\tau} \tag{2}$$

If the system is periodically driven for a long time, it will asymptotically reach a limit cycle or a time-periodic solution $\vec{p}(t) = \vec{p}(t+\tau)$. For this periodic steady state, let us define a scaled time

$$h = \frac{t}{\tau} \tag{3}$$

and

$$\vec{\rho}(h) = \vec{p}(h\tau) \tag{4}$$

The corresponding master equation is written as

$$\frac{\mathrm{d}\vec{\rho}(h)}{\mathrm{d}h} = \tau\tilde{R}_h\vec{\rho}(h) \tag{5}$$

where $\tilde{R}_h = \hat{R}_{h\tau}$.

Now consider the fast oscillation limit, the size of the limit cycle will shrink into a single point, yielding an *effective steady state probability*, $\vec{\rho}_0$. This effective steady state is denoted by $\vec{p}^*$ in the main text. To show this, let us perform perturbation analysis by expanding $\vec{\rho}(h)$ into

$$\vec{\rho}(h) = \sum_{n=0}^{\infty}\tau^n\vec{\rho}_n(h) \tag{6}$$

In the limit $\tau \to 0$, by plugging Eq. 6 into Eq. 5 and matching terms at different order of τ, we obtain:

$$\frac{\mathrm{d}\vec{\rho}_0(h)}{\mathrm{d}h} = 0 \tag{7}$$

$$\frac{\mathrm{d}\vec{\rho}_1(h)}{\mathrm{d}h} = \tilde{R}_h\vec{\rho}_0 \tag{8}$$

where h ranges from 0 to 1 during one period. Since the system is at a periodic steady state $\vec{\rho}(0) = \vec{\rho}(1)$ for any τ, all orders must satisfy $\vec{\rho}_n(0) = \vec{\rho}_n(1)$.

According to Eq. 7, $\vec{\rho}_0(h)$ is a stationary point independent of h. Thus by integrating Eq. 8 over a whole period (h from 0 to 1), we can find

$$\vec{\rho}_1(1) - \vec{\rho}_1(0) = \left(\int_0^1 \mathrm{d}h\tilde{R}_h\right)\vec{\rho}_0 \tag{9}$$

* zhiyuelu@unc.edu

Thus, we can find that the effective stationary state $\vec{p}^* = \vec{\rho}_0$ is the stationary solution for an time-averaged rate matrix $\hat{R}^*$:

$$0 = \left(\int_0^1 \mathrm{d}h\tilde{R}_h\right)\vec{\rho}_0 = \frac{1}{\tau}\left(\int_0^\tau \mathrm{d}t\hat{R}_t\right)\vec{p}^* = \hat{R}^*\vec{p}^* \tag{10}$$

where the time averaged rate matrix is defined by

$$\hat{R}^* = \frac{1}{\tau}\int_0^\tau \mathrm{d}t\hat{R}_t \tag{11}$$

II. ALTERNATIVE DERIVATION OF THE UNIVERSAL OBJECTIVE FUNCTION

In this section, we demonstrate an alternative derivation of the central result, starting by assuming small amplitude of temperature oscillation, where the inverse temperature oscillates around β_0. The ability to invert reaction is characterized by the change of thermodynamic driving force, which is characterized by $\Delta\tilde{\mathcal{A}}$. $\Delta\tilde{\mathcal{A}}$ is the value difference of $\tilde{\mathcal{A}}(\mathbf{r})$ between points O and D in Fig. 2 of the main text. Notice that $\Delta\tilde{\mathcal{A}}$ reflects the local curvature-like property of the β-locus around any β_0 and it mainly depends on the catalyst's energy landscape $\{\alpha_{ij}\}$. Thus we can derive a generic energy landscape optimization principle independent of the temperature protocol. Let us start by expressing $\Delta\tilde{\mathcal{A}}$ as

$$\Delta\tilde{\mathcal{A}} = \tilde{\mathcal{A}}(\hat{R}^*) - \tilde{\mathcal{A}}(\hat{R}_0) = \sum_{\langle i,j\rangle}\varepsilon_{ij}\log\frac{R^*_{ij}}{R_{0,ij}} \tag{12}$$

By plugging in the Arrhenius Law

$$R_{ij}(\beta_0 \pm \Delta\beta) = r_{ij,0}\exp[-(\beta_0 \pm \Delta\beta)\alpha_{ij}] \tag{13}$$

$$= \exp(\mp\alpha_{ij}\Delta\beta)R_{ij}(\beta_0) \tag{14}$$

Thus

$$R^*_{ij} = \frac{R_{ij}(\beta_0+\Delta\beta) + R_{ij}(\beta_0-\Delta\beta)}{2} \tag{15}$$

$$= \cosh(\alpha_{ij}\Delta\beta)R_{ij}(\beta_0) \tag{16}$$

When $\Delta\beta \to 0$,

$$\log\cosh(\alpha_{ij}\mathrm{d}\beta) = \frac{1}{2}\alpha_{ij}^2\mathrm{d}\beta^2 + o(\mathrm{d}\beta^2) \tag{17}$$

In the end, $\Delta\tilde{\mathcal{A}}$ is dictated by a local curvature-like property as

$$\Delta\tilde{\mathcal{A}} = \sum_{\langle i,j\rangle}\varepsilon_{ij}\log\cosh(\alpha_{ij}\mathrm{d}\beta) \tag{18}$$

$$= \frac{1}{2}\sum_{\langle i,j\rangle}\varepsilon_{ij}\alpha_{ij}^2\mathrm{d}\beta^2 + o(\mathrm{d}\beta^2) \tag{19}$$

This derivation leads to the objective function as Eq. 13 in the main text that can be used to predict the performance of the catalyst:

$$\mathcal{C} \equiv \sum_{\langle i,j\rangle}\varepsilon_{ij}\alpha_{ij}^2 \tag{20}$$

III. SOLVING CURRENT AT FAST OSCILLATION LIMIT

At the fast oscillation limit $f \gg 1$, the reaction current J_{period} can be analytically solved by using the Matrix Tree Theorem[2]. For a 3-state ring, the current can be expressed as

$$J^* = \frac{R^*_{13}R^*_{32}R^*_{21} - R^*_{12}R^*_{23}R^*_{31}}{\kappa} \tag{21}$$

where the denominator is positive: $\kappa = R^*_{12}R^*_{13} + R^*_{13}R^*_{21} + R^*_{12}R^*_{23} + R^*_{21}R^*_{23} + R^*_{12}R^*_{31} + R^*_{23}R^*_{31} + R^*_{13}R^*_{32} + R^*_{21}R^*_{32} + R^*_{31}R^*_{32}$. The net current J^* shares the same sign with the effective driving force $\tilde{\mathcal{A}}^* = \log(R^*_{13}R^*_{32}R^*_{21}) - \log(R^*_{12}R^*_{23}R^*_{31})$ at the fast limit. This result is directly applicable to N-state rings.

IV. SOLUTION TO THE OPTIMIZATION PROBLEM

Here we demonstrate the steps needed to find the optimal energy landscape for the 3-state catalytic cycle. Within the cycle, there are 3 forward transitions whose activation energies are denoted by α_1, α_2, and α_3, and 3 backward transitions whose activation energies are denoted by α_4, α_5, α_6. To find the strongest energy landscape for chemical reaction inversion is equivalent to searching for the values of α_1 to α_6 such that the cost function

$$\mathcal{C} = \alpha_1^2 + \alpha_2^2 + \alpha_3^2 - (\alpha_4^2 + \alpha_5^2 + \alpha_6^2) \tag{22}$$

is minimized under the constraints that

$$(\alpha_4 + \alpha_5 + \alpha_6) - (\alpha_1 + \alpha_2 + \alpha_3) = 1 \tag{23}$$

and that

$$0 \leq \alpha_i \leq \alpha_{\max} \tag{24}$$

for $i = 1, 2, \cdots 6$.

It is intuitive to separately deal with the forward activation energies and the backward activation energies for the above optimization problem. Here let us introduce a function conditioned on s:

$$f(x, y, z; s) = x^2 + y^2 + z^2 \tag{25}$$

where the condition is that $x + y + z = s$. Then, the optimization problem under the restrictions listed above can be broken into two steps, first optimize $\mathcal{C}$ under a given value of $s = \alpha_4 + \alpha_5 + \alpha_6$ and equivalently $s - 1 = \alpha_1 + \alpha_2 + \alpha_3$, and then vary the value of s to find the desired optimum. In other words, the optimization is obtained by solving

$$\inf_s(\inf_{\alpha_1,\alpha_2,\alpha_3} f(\alpha_1, \alpha_2, \alpha_3; s-1) - \sup_{\alpha_4,\alpha_5,\alpha_6} f(\alpha_4, \alpha_5, \alpha_6; s)) \tag{26}$$

Notice that the $\inf_{\alpha_1,\alpha_2,\alpha_3} f(\alpha_1, \alpha_2, \alpha_3; s-1)$ can be found at $((s-1)/3, (s-1)/3, (s-1)/3)$ despite the restriction that $0 \leq x, y, z \leq \alpha_{\max}$. (Notice that we have decided that $\alpha_{\max} > \mathcal{A} = 1$.) However the $\sup_{\alpha_4,\alpha_5,\alpha_6} f(\alpha_4, \alpha_5, \alpha_6; s)$ lies on the boundary of the intersection between the cube $0 \leq x, y, z \leq \alpha_{\max}$ and the plane $x + y + z = s$. Thus the sup depends on the choice of s:

$$\arg\max_{\alpha_4,\alpha_5,\alpha_6} f(\alpha_4, \alpha_5, \alpha_6; s) = \begin{cases} (s, 0, 0) & 0 \leq s \leq \alpha_{\max} \\ (\alpha_{\max}, s - \alpha_{\max}, 0) & \alpha_{\max} < s \leq 2\alpha_{\max} \\ (\alpha_{\max}, \alpha_{\max}, s - 2\alpha_{\max}) & 2\alpha_{\max} < s \leq 3\alpha_{\max} \end{cases} \tag{27}$$

Then we found that since we allowed for $\alpha_{\max} > 1$, the minimum is taken at $s = 2\alpha_{\max}$,

$$\alpha_+ = (\frac{2\alpha_{\max} - 1}{3}, \frac{2\alpha_{\max} - 1}{3}, \frac{2\alpha_{\max} - 1}{3}) \tag{28}$$

$$\alpha_- = (\alpha_{\max}, \alpha_{\max}, 0) \tag{29}$$

[1] M. Tagliazucchi, E. A. Weiss, and I. Szleifer, Dissipative self-assembly of particles interacting through time-oscillatory potentials, Proceedings of the National Academy of Sciences **111**, 9751 (2014).

[2] J. Schnakenberg, Network theory of microscopic and macroscopic behavior of master equation systems, Reviews of Modern physics **48**, 571 (1976).